Front. Earth Sci. 2022, 16(2): 277–290
https://doi.org/10.1007/s11707-020-0854-9

RESEARCH ARTICLE

Effects of local and non-local closure PBL schemes on the simulation of Super Typhoon Mangkhut (2018)

Zixi RUAN[1,2], Jiangnan LI (✉)[1,2], Fangzhou LI[1], Wenshi LIN[1]

1 School of Atmospheric Sciences, and Guangdong Province Key Laboratory for Climate Change and Natural Disaster Studies, Sun Yat-sen University, Zhuhai 519082, China
2 Southern Marine Science and Engineering Guangdong Laboratory (Zhuhai), Zhuhai 519082, China

Abstract With the convection-permitting simulation of Super Typhoon Mangkhut (2018) with a 3 km resolution for 10.5 days using mesoscale numerical model, Weather Research and Forecasting Model Version 4.1 (WRFV4.1), the influences of local closure QNSE planetary boundary layer (PBL) scheme and non-local closure GFS planetary boundary layer scheme on super typhoon Mangkhut are mainly discussed. It is found that in terms of either track or intensity of typhoon, the local closure QNSE scheme is better than the non-local closure GFS scheme. Local and non-local closure PBL schemes have a large influence on both the intensity and the structure of typhoon. The maximum intensity difference of the simulated typhoon is 50 hPa. The intensity of typhoon is closely related to its variations in structure. In the rapid intensification stage, the typhoon simulated by the QNSE scheme has a larger friction velocity, stronger surface latent heat flux, sensible heat flux and vapor flux, related to a higher boundary height and stronger vertical mixing. The latent heat flux and sensible heat flux on the surface conveyed energy upward for the typhoon while the water vapor was transported upward through vertical mixing. While the water vapor condensed, the latent heat was released, which further warmed the typhoon eyewall, strengthening the convection. The stronger winds also intensified the vertical mixing and the warm-core structure, further strengthened the typhoon. The differences in surface layer schemes dominated the differences between the two simulations.

Keywords typhoon, planetary boundary layer scheme, WRF model

Received May 20, 2020; accepted November 26, 2020

E-mail: essljn@mail.sysu.edu.cn

1 Introduction

In the planetary boundary layer (PBL), the vertical transportations of water vapor, kinetic energy, and heat are implemented under the action of turbulence. For there are different methods applied to process turbulence closure problems, PBL parameterization schemes are divided into local and non-local schemes. Local closure means that the variables in each layer and the gradients of these variables are used to calculate the pulsating flux and the pulsating flux on each grid point depends entirely on the average of the variables on the gird point; for example, the local K theory (Pleim and Chang, 1992) and the turbulent kinetic energy closure method (Yamada and Mellor, 1975). As for the non-local closure, an unknown variable of grid point is parameterized by the known variable at many points and the calculation of the pulsating flux on each grid point is comprehensively influenced by the grid point and the other grid points surrounding it; for example, the non-local K theory (Deardorff, 1972), the transient turbulence theory, and the general diffusion theory. Different schemes have different turbulent diffusion equations.

The PBL scheme is a key factor influencing the intensity of tropical cyclone (TC) (Li and Pu, 2008; Ricchi et al., 2017). The TC intensity depends primarily on the surface flux rather than the vertical mixing (Braun and Tao, 2000). The TC intensity changes along with the enthalpy–momentum exchange coefficient and the surface roughness (Emanuel, 1995; Braun and Tao, 2000). However, Liu et al. (2017) found that both the surface flux and the vertical mixing of the PBLs had a significant impact on forecasts of the TC intensity. The different turbulent diffusion coefficients of the different PBL schemes can result in different TC intensities (Smith and Thomsen, 2010). The different PBL schemes reflect the diverse characteristics of the PBL (Nolan et al., 2009a, 2009b). In

addition to vertical diffusion, horizontal diffusion in the PBLs also plays a critical role in simulating the hurricane intensity (Rotunno and Bryan, 2012). The simulated TC intensity is sensitive to the ratio of the enthalpy to the momentum (Ooyama, 1969). Zhang et al. (2017) pointed out that a lower vertical vorticity diffusion coefficient corresponded to better TC simulations, which emphasizes the major function of the PBL structure on variations in the TC intensity.

In summary, the influence of PBL schemes on simulated typhoon is still uncertain in many aspects such as seasonal and regional differences and applicability (Efstathiou et al., 2013; Zhang et al., 2013; Tymvios et al., 2018; Sun and Li, 2018). The physical factors and processes of how the different schemes influence the simulated TCs are also diverse. For example, turbulent diffusion coefficients, surface flux calculation methods, and the ratio of the enthalpy to the momentum, can all affect the simulation. That is, such uncertainties give rise to large differences in the TC tracks, intensities, and structures forecasted by different schemes (Deng et al., 2005; Smith and Thomsen, 2010; Wang et al., 2017; Xu et al., 2017; Wen et al., 2018).

As seen in previous studies of PBL structures, local closure schemes generated better simulation under stable conditions; however, under unstable situations, non-local closure schemes were superior (Huang et al., 2014). The environment of typhoon continuously changes between stable and unstable conditions. Investigations of the influence of local and non-local closure schemes on simulated typhoon have rarely been implemented. For this reason, this study focused on analyzing the influence of these two categories of PBL schemes on the typhoon intensity based on contrasting tests performed by a local closure scheme and a non-local closure scheme.

At present, numerical predictions or simulation researches of typhoons are mainly limited within 1–5 days. The simulation research of typhoons for more than 10 days in this paper is an exploratory and innovative task, which has important reference value for the short-term climate prediction of typhoons. Thus, in this paper, non-local closure GFS scheme and turbulent kinetic energy closure QNSE scheme were used for simulation. To avoid the influence of cumulus parameterization schemes, we designed two high-resolution convection-permitting experiments without cumulus parameterization schemes. The major purpose was to compare the simulated short-term climate of the typhoon using two different boundary layer schemes.

The next section briefly summarizes an overview of Typhoon Mangkhut (2018). Section 3 covers the experimental design. Section 4 provides a comparison of the simulation results. Section 5 demonstrates different effects of the PBL schemes on the typhoon intensity. Finally, conclusions and discussion are given.

2 Overview of Typhoon Mangkhut (2018)

At 00:00 on 7 September, 2018 (UTC, the same below), Japan Meteorological Agency upgraded the tropical disturbance generated over the north-west Pacific Ocean to a tropical depression. After 13 h and 15 min, it was upgraded to a tropical storm and named “Mangkhut”. Typhoon Mangkhut strengthened rapidly, moved west by north, and became a violent typhoon at 06:00 on 10 September and super typhoon at 00:00 on 11 September. It reached its maximum at 12:00 on 11 September. At this time, its minimum sea level pressure (MSLP) was 910 hPa and its maximum surface wind (MSW, defined by maximum 10 m wind) was 65 m/s. It landed from Luzon at 17:40 on 14 September as a super typhoon and abated then. At 00:00 on 15 September, it moved to the South China Sea and weakened into a strong typhoon. After entering the South China Sea, the Typhoon Mangkhut continued moving to the north-west with invariant strength. It landed in Taishan, Guangdong on 16 September with the maximum wind of force 14 near the typhoon center at the time of landfall. After the landfall, Mangkhut was weakened rapidly and became a tropical depression while it moved to Guangxi and then gradually dissipated.

Typhoon Mangkhut affected nearly 3 million people in Guangdong, Guangxi, Hainan, Hunan, and Guizhou provinces, leaving five people dead and one missing. More than 1200 houses collapsed and 174.4 million hectares of crops were affected, resulting in a direct economic loss of 5.2 billion yuan.

3 Data and experimental design

The ERA-Interim reanalysis data of the European Center for Medium-Range Weather Forecasts (ECMWF) at a resolution of $0.125° \times 0.125°$ were used as the initial field data for the model simulation. The best track data from China Meteorological Administration (CMA) Tropical Cyclone Database was used to compare with simulation results (Ying et al., 2014). The simulation was performed by the mesoscale numerical model Advanced Research WRF Version 4.1 (WRF-ARW4.1) using the Mercator projection. The simulated time period is from 00:00 on 7 September 2018 to 12:00 on 17 September 2018, covering a total of 10 days and 12 h (basically covering the process of Mangkhut from tropical depression to extinction) with the spatial resolution of 3 km and the horizontal grid of 921×2101 (Experiments domain setting in WRF model can be found from electronic supplementary material). The model had a top pressure of 50 hPa and 39 σ layers with unequal distances were selected vertically. WSM7 cloud micro-physical scheme (Bae et al., 2019), unified NOAH

land surface scheme (Tewari et al., 2004), RRTM long-wave radiation scheme (Mlawer et al., 1997), Dudhia short-wave radiation scheme (Dudhia, 1989) were adopted. No cumulus parameterization scheme was activated. To explore the influence of local and non-local closure PBL schemes on the simulation of Mangkhut, two experiments were conducted by selecting a local closure QNSE scheme with a corresponding QNSE surface layer scheme (named as QNSE-EXP) (Sukoriansky et al., 2005) and a non-local closure GFS scheme with a corresponding GFS surface layer scheme (named as GFS-EXP) (Hong and Pan, 1996), respectively.

In the QNSE scheme, the turbulent kinetic energy closure scheme of MYJ (Janjić, 2002) was adopted under unstable stratification (Mellor and Yamada, 1982); the QNSE scheme had good performance under stable stratification. The K-ε model developed from turbulence spectrum closure model was adopted. This model improved the MYJ scheme of momentum and heat diffusion coefficient formula and kept the physical process closer to the actual atmosphere. It not only distinguished explicitly the difference in quality caused by the stratification between horizontal and vertical transportations but also considered the mutual effect between turbulence and wave (Sukoriansky, 2005). The non-local closure GFS scheme is based on Troen and Mahrt (1986), Holtslag and Moeng (1991), as well as the non-local diffusion methods by Holtslag and Boville (1993). The non-local closure method can better represent the large vortex flux of the mixed layer; the local diffusion method is used for diffusion in the free atmosphere (Hong and Pan, 1996).

4 Results

4.1 Track

Each boundary layer scheme can well simulate the track of Typhoon Mangkhut (Fig. 1). From 24 h to 84 h after typhoon was formed, the two schemes fit well, then the typhoon track in QNSE-EXP was obviously closer to the best track than that in GFS-EXP. At the beginning of the simulation, an error comparison was made every 24 h as shown in Fig. 2. Both the distance and angel errors in QNSE-EXP were larger in the first 48 h than those in GFS-EXP. However, the track error in QNSE-EXP was smaller than that simulated by the GFS scheme since then. Positive values indicated that the simulated position deviated to the

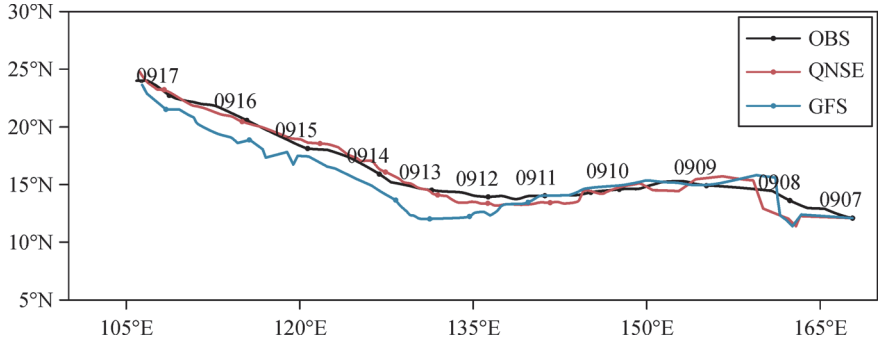

Fig. 1 Comparison of the simulated track of TC with observation (OBS) based on the CMA's TC database.

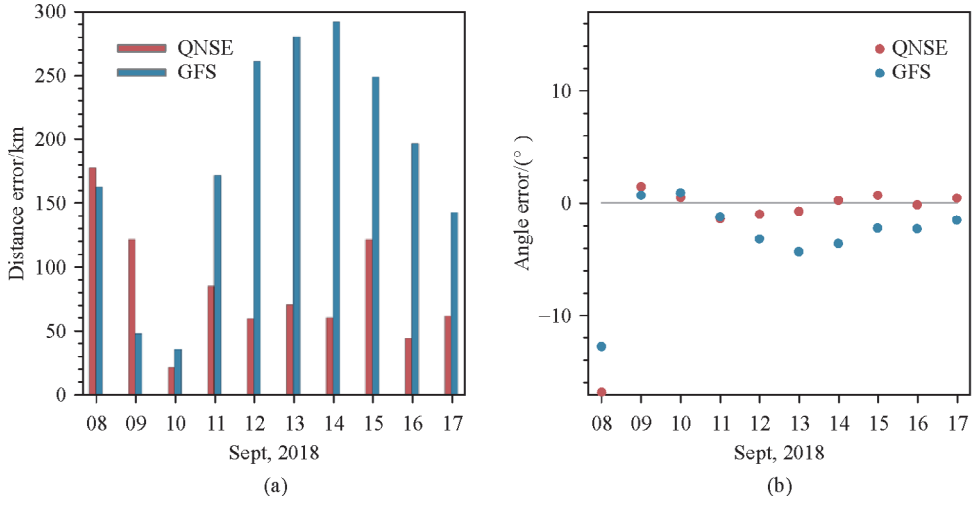

Fig. 2 (a) Simulated distance error (left, unit: km) and (b) angle error (right, unit: °).

right, while negative values indicated that the simulated position deviated to the left (Fig. 2(b)). In the early stage, all errors of both schemes were very large. After the initial adjustment, the moving direction error and track error in QNSE-EXP gradually decreased, while those in GFS-EXP decreased a little and then began to increase. QNSE scheme has better performance on simulating the typhoon track.

4.2 Intensity

The variation trend of typhoon intensity simulated by the two schemes was basically consistent with the best track (Fig. 3). Both of them intensified rapidly in the early stage, then remained unchanged in a period, decreased rapidly, remained unchanged for a short time, and finally weakened rapidly and dissipated. However, the simulation intensities using the two schemes were quite different. The two schemes slightly lagged behind the best track in the early stage of typhoon intensification. After adjustment, the typhoon in QNSE-EXP began to strengthen rapidly at around 00:00 on 10 September 2018, which was closer to the observation, while that in GFS-EXP also started to strengthen with a lesser intensification speed. The maximum intensity was 910 hPa. The simulation results were 914 hPa using QNSE scheme and 963 hPa using GFS scheme, respectively.

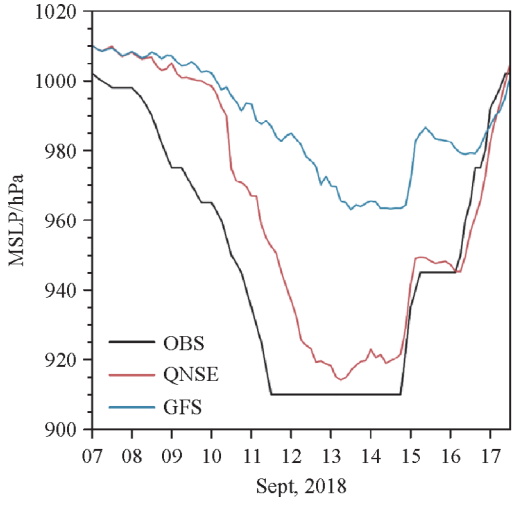

Fig. 3 Comparison of simulated minimum sea level pressure of TC with observation.

Correlation coefficients (*R*), bias (*BIAS*), normalized bias (*NBIAS*), root mean square error (*RMSE*), and normalized root mean square error (*NRMSE*) were used to assess the simulated typhoon intensity using two PBL schemes. Their calculation formulas are Eqs. (1)–(5). F_i and O_i represent variables (*MSLP* or *MSW*) of simulations and the observation, respectively.

$$R = \frac{\sum_{i=1}^{N}(F_i-\overline{F})(O_i-\overline{O})}{\sqrt{\sum_{i=1}^{N}(F_i-\overline{F})^2}\sqrt{\sum_{i=1}^{N}(O_i-\overline{O})}}, \quad (1)$$

$$BIAS = \frac{1}{N}\sum_{i=1}^{N}(F_i-O_i), \quad (2)$$

$$NBIAS = \frac{\sum_{i=1}^{N}(F_i-O_i)}{\sqrt{\sum_{i=1}^{N}(O_i-\overline{O})^2}} \times 100\%, \quad (3)$$

$$RMSE = \sqrt{\frac{1}{N}\sum_{i=1}^{N}(F_i-O_i)^2}, \quad (4)$$

$$NRMSE = \frac{\sqrt{\sum_{i=1}^{N}(F_i-O_i)^2}}{\sqrt{\sum_{i=1}^{N}(O_i-\overline{O})^2}} \times 100\%. \quad (5)$$

QNSE-EXP had a larger correlation coefficient and smaller errors compared with the observation than that in GFS-EXP (Table 1). The QNSE scheme performed closer to the observation than the GFS scheme in the early stage, which was consistent with Wen et al. (2018) indicating that the QNSE scheme could better simulate the formation and development of tropical disturbance in the boundary layer in the initial stage of the typhoon.

As for MSW (Fig. 4), the variation trends simulated by the two schemes were basically consistent with the observation. In the early stage, the simulated MSW of the two schemes was close to the observation. When the typhoon reached its maximum, the MSW was 65 m/s, the MSW in QNSE-EXP was 59.2 m/s, while that in GFS-EXP was 47.7 m/s. As shown in Table 2, the simulation using QNSE scheme also had a better correlation with the observation with smaller errors.

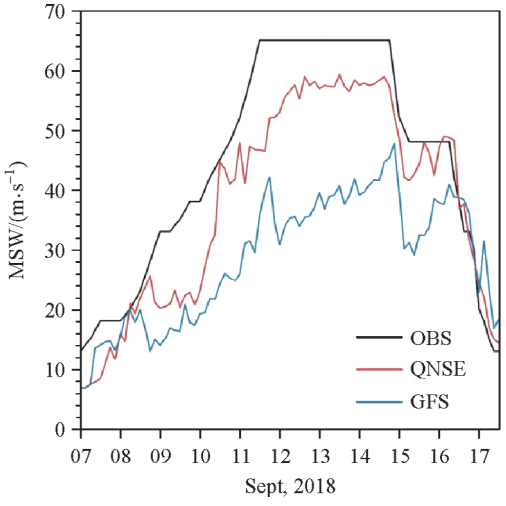

Fig. 4 Comparison of simulated maximum surface wind of TC with observation.

Table 1 Assessment statistics of simulated minimum sea level pressure of TC

Assessment	QNSE	GFS
R	0.919496	0.83056
BIAS/hPa	−14.0431	−38.0171
NBIAS/%	−1.47856	−4.00272
RMSE/hPa	19.5743	44.3034
NRMSE/%	2.06083	4.66459

Table 2 Assessment statistics of simulated maximum surface wind of TC

Assessment	QNSE	GFS
R	0.955226	0.823218
BIAS/(m·s^{-1})	6.64404	15.9988
NBIAS/%	14.9462	35.9904
RMSE/(m·s^{-1})	8.556	19.5313
NRMSE/%	19.2473	43.9371

5 Mechanism of the influence of PBL scheme on typhoon intensity

Based on the analysis above, it can be seen that the local closure QNSE boundary layer parameterization scheme and the non-local closure GFS scheme had impact on the track and intensity simulation of the typhoon, especially on the typhoon intensity. The difference of the maximum simulated typhoon intensity was 50 hPa. To explore the mechanism of the influence by different boundary layer schemes on typhoon intensity, the surface fluxes and vertical structure of typhoons were analyzed.

According to the rapid intensification stage of typhoon defined by Kaplan and DeMaria (2003), the stage of Typhoon Mangkhut from 00:00 on 10 September 2018 to 12:00 on 11 September 2018 can be classified as the stage of rapid intensification of the typhoon. When the typhoon reached its maximum, the minimum pressure in the center was 910 hPa, and the MSW near the typhoon center was 65 m/s. The two boundary layer schemes simulated the typhoon intensification stage with hysteresis, so this paper analyzed the stage from 00:00 on 10 September to 00:00 on 13 September 2018 as the typhoon rapid intensification stage.

5.1 Surface flux

The intensity of hurricane simulation is largely dependent on surface flux rather than vertical mixing (Braun and Tao, 2000). In the WRF model, the surface fluxes are calculated by surface layer schemes (Filippos et al., 2018). As can be seen from Fig. 5, the typhoon in QNSE-EXP had significantly stronger surface fluxes, larger friction velocity, and higher PBL height than that in GFS-EXP. The surface fluxes in QNSE-EXP had similar trends, the variables first increased rapidly over time and then decreased after reaching the peak at around 12:00 on 10 September, 2018, and then continued to increase, showing an overall increasing trend. The surface friction velocity and PBL height simulated in QNSE-EXP had a similar rapidly increasing trend. However, the five variables in GFS-EXP increased slowly over time, with the variation trend more gradual and the values much smaller compared to those in QNSE-EXP. On the whole, the latent heat flux (Fig. 5(b)) was one order of magnitude larger than the sensible heat flux, especially during the mature period (Fig. 6(a)). Therefore, the latent heat flux was the main source of typhoon energy. Water vapor condensation released latent heat and provided energy for the typhoon, while the variation trend of the surface water vapor flux (Fig. 5(c)) was consistent with those of the surface sensible heat flux (Fig. 5(a)) and surface latent heat flux (Fig. 5(b)). The water vapor flux in QNSE-EXP was larger than that in GFS-EXP. In QNSE-EXP, the simulated surface friction velocity was between 0.6 and 2.2 m/s and PBL height was between 1.5 and 5 km, while in GFS-EXP, the simulated surface friction velocity was between 0.4 and 1.2 m/s and PBL height was below 2 km.

The friction velocity, the Obukhov length scale, and PBL height are important in atmospheric stable boundary layer (Sukoriansky et al., 2005). The stress also plays a major role in the boundary layer of hurricanes (Moss and Rosenthal, 1975). Surface friction velocity is related to surface stress and vertical momentum flux, so larger surface friction velocity induces stronger vertical mixing (Deng et al., 2005). The PBL height simulated by QNSE scheme is defined as a level at which the turbulent momentum flux falls to 5% of its surface value (Sukoriansky et al., 2005). Therefore, the stronger vertical turbulent mixing shows the higher PBL height. The PBL height simulated by GFS scheme is given by Eq. (6), where Rib_{cr} is the critical bulk Richardson number, $U(h)$ is the horizontal wind speed at h, θ_{va} is the virtual potential temperature at the lowest model level, $\theta_{\mathrm{v}}(h)$ is the virtual potential temperature at h, and θ_{s} is the appropriate temperature near the surface (Hong and Pan, 1996).

$$h = Rib_{\mathrm{cr}}\frac{\theta_{\mathrm{va}}|U(h)|^2}{g(\theta_{\mathrm{v}}(h)-\theta_{\mathrm{s}})}. \tag{6}$$

These two schemes have different vertical diffusion processes. The QNSE scheme uses the 1.5-order turbulence closure model and provides expressions for the horizontal and vertical turbulent viscosities and diffusivities, considering the interaction of waves and turbulence in stable boundary layer (Sukoriansky et al., 2005). While GFS scheme uses non-local closure approach in well-mixed layer, and the countergradient term is important in

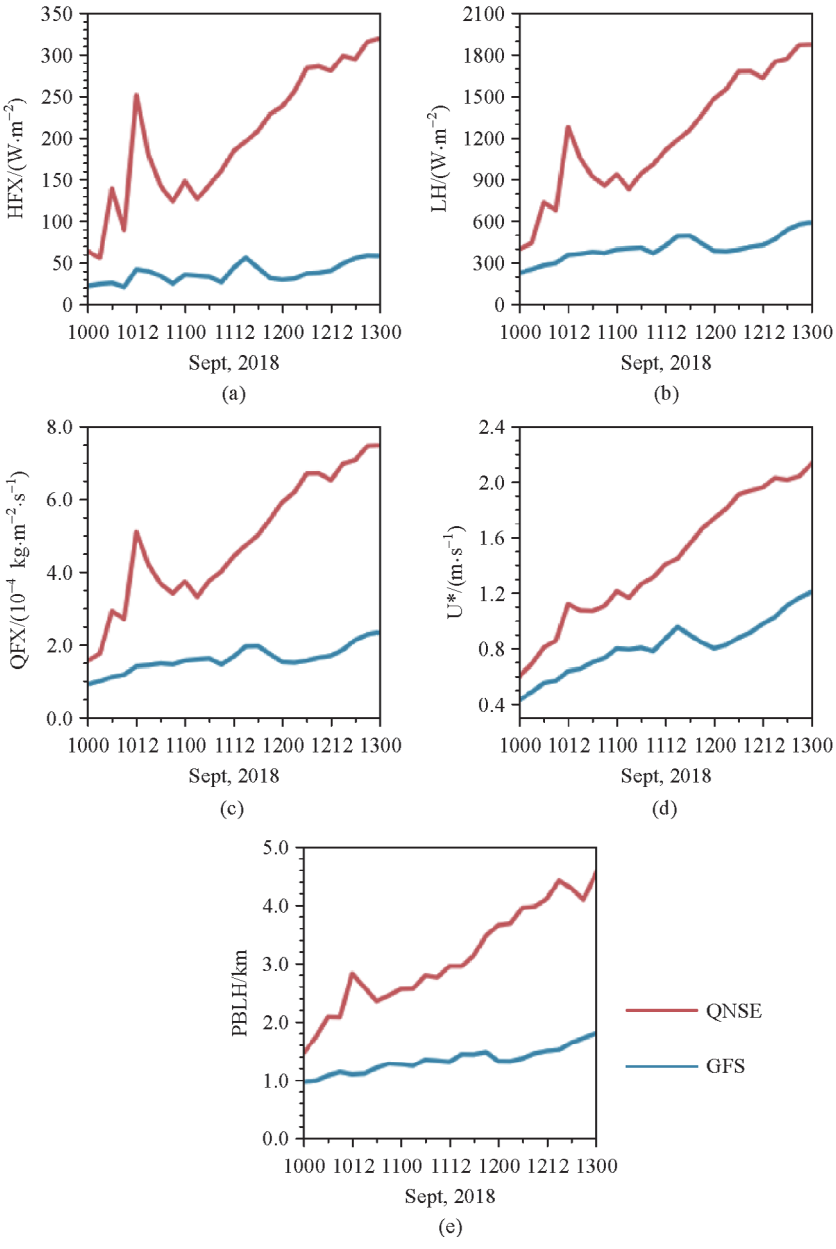

Fig. 5 Time variation of simulated regional average (within a radius of 150 km from TC center). (a) Surface sensible heat flux (HFX), (b) surface latent heat flux (LH), (c) surface water vapor flux (QFX), (d) surface friction velocity (U*) and (e) boundary layer height (PBLH) during the mature stage (from 00:00 of 10th to 00:00 of 13th, the same below).

stabilizing the mixed layer and transporting the surface moisture upward (Hong and Pan, 1996). Under stronger vertical mixing, the surface fluxes could be rapidly transported to a higher level, leading to much greater energy of the typhoon. Thus, the typhoon intensity in QNSE-EXP was stronger than that in GFS-EXP, which was consistent with the previous simulation results of the typhoon intensity.

The surface sensible heat flux has both positive and negative values (Fig. 6). The positive values represent the upward sensible heat flux, which can promote the development and maintenance of typhoons. The sensible heat flux in QNSE-EXP was more than 1200 W/m^2, much stronger than that in GFS-EXP. The sensible heat fluxes simulated in both two schemes were positive in the typhoon main body, the weakest in the typhoon center, and gradually strengthened outward. After reaching the strongest near the eyewall, it gradually weakened outwards, with the weak negative sensible heat fluxes over the typhoon periphery. The strongest sensible heat flux in QNSE-EXP was located in the north-east near the typhoon center, while that in GFS-EXP was located in the north-west near the typhoon center. There was a strong sensible heat flux area corresponding to the spiral cloud belt. As a

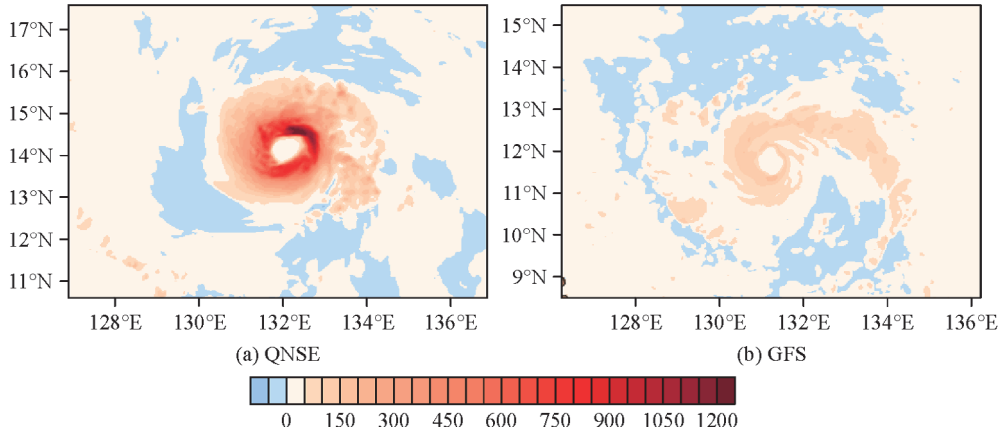

Fig. 6 Simulated surface sensible heat fluxes (unit: W/m^2) of TC at 00:00 on 13 September, 2018.

whole, the sensible heat flux simulated by QNSE scheme was significantly stronger than that simulated by GFS scheme.

It can be seen from Fig. 7 that the latent heat fluxes simulated by the two schemes were the weakest in the center of typhoon, gradually increasing outwards, and gradually weakening outwards after reaching the strongest near the eye wall. The strongest area of latent heat flux simulated by QNSE scheme was located in the north-east quadrant of typhoon, similar to the distribution of sensible heat flux (Fig. 6(a)), which was more than 5600 W/m^2. The strongest latent heat flux simulated by GFS scheme was less than 1200 W/m^2, located in the north and south of typhoon eye area and near the spiral rain belt near the typhoon wall on the north side, which was a bit different from the distribution of sensible heat flux (Fig. 6(b)). The latent heat flux simulated by QNSE scheme was stronger than that simulated by GFS scheme, with the strongest latent heat flux near the eye wall area in QNSE-EXP 5 times higher than that in GFS-EXP. The simulated latent heat flux was almost 5 times higher than the simulated sensible heat flux in both schemes. Latent heat played a more important role in development of typhoon, which was in agreement with Ding et al. (2018).

The distribution of surface water vapor flux (Fig. 8) was similar to that of latent heat flux (Fig. 7). The water vapor flux in the center of typhoon was basically zero, gradually increasing outwards, reaching the strongest in the eyewall, and then gradually weakening outwards. The strongest area of simulated water vapor transport was basically the same as that of latent heat flux. The water vapor condensed to release latent heat. Therefore, the distribution of water vapor flux and latent heat flux was the same. The strongest water flux was 22×10^{-4} kg·m^{-2}·s^{-1} in QNSE-EXP and 6×10^{-4} kg·m^{-2}·s^{-1} in GFS-EXP. The simulated water vapor flux in QNSE-EXP was much stronger than that in GFS-EXP, which indicates more water vapor transported to the typhoon eyewall, more latent heat released by water vapor, more energy obtained by typhoon, and hence a stronger typhoon intensity.

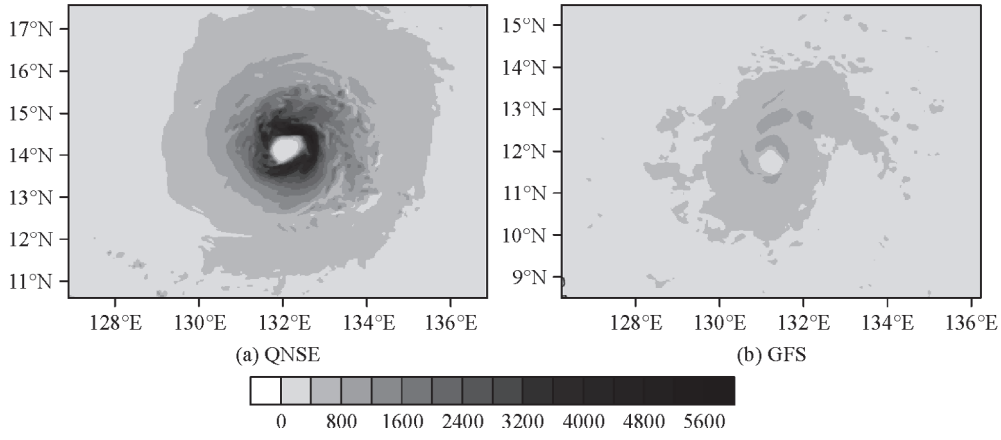

Fig. 7 Simulated surface latent heat fluxes (unit: W/m^2) of TC at 00:00 on 13 September, 2018.

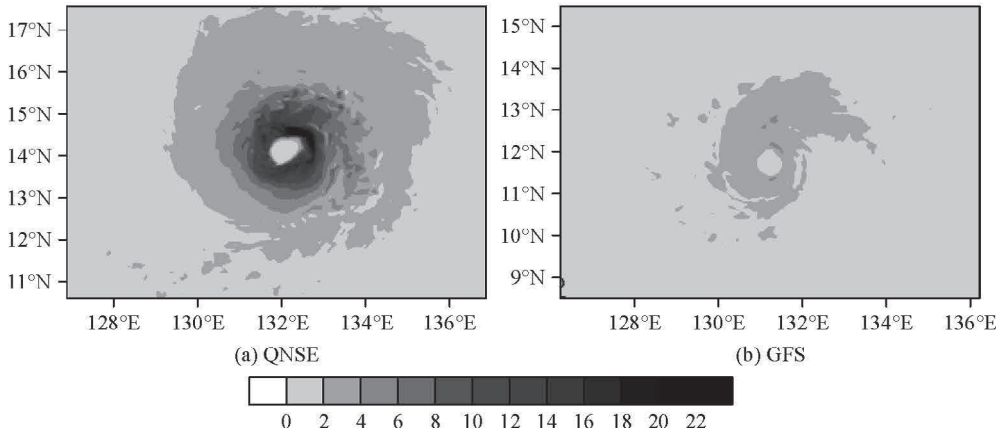

Fig. 8 Simulated water vapor fluxes (unit: 10^{-4} kg·m^{-2}·s^{-1}) of TC at 00:00 on 13 September, 2018.

5.2 Vertical mixing and structure

Local QNSE scheme and non-local GFS scheme have different vertical diffusion processes. The vertical velocities simulated by the two schemes had a vertical sinking motion in the typhoon center (Fig. 9). The adiabatic heating of sinking airflow played an important role in maintaining the warm-core structure in the typhoon eye region. The strongest ascending velocity was found at the eyewall of the typhoon. The ascending air flow presented the characteristics of inclining outwards with the height. The QNSE scheme simulated the subsidence movement below 18 km near the typhoon center with the maximum vertical speed of 1 m/s, while the GFS scheme mainly simulated the subsidence movement at the height of 8–14 km near the typhoon center with the maximum vertical speed of 0.8 m/s. The maximum vertical updraft velocity of the eyewall in QNSE-EXP was found at the radius of 50 km and the altitude of 4 km, corresponding to the size of the simulated typhoon eye (Fig. 6(a)). The maximum vertical updraft velocity reached 2 m/s. The maximum value in GFS-EXP was found at the radius of 60 km and the height of 12 km while the maximum vertical updraft velocity only reached 0.6 m/s. Whether the sinking speed or the rising speed, the QNSE scheme simulated larger than the GFS scheme. The subsidence movement induced adiabatic descent leading to the temperature increasing in the center of typhoon. The height of vertical movement was simulated also higher by the QNSE scheme than the GFS scheme, indicating that the QNSE scheme simulated more severe typhoon convection and stronger typhoon intensity.

Tangential wind embodied the characteristics of the main circulation of the typhoon. As can be seen from Fig. 10, the tangential wind was simulated obviously stronger in QNSE-EXP than in GFS-EXP. And the tangential wind in QNSE-EXP reached at a higher level than that in GFS-EXP. That is, the height of the main

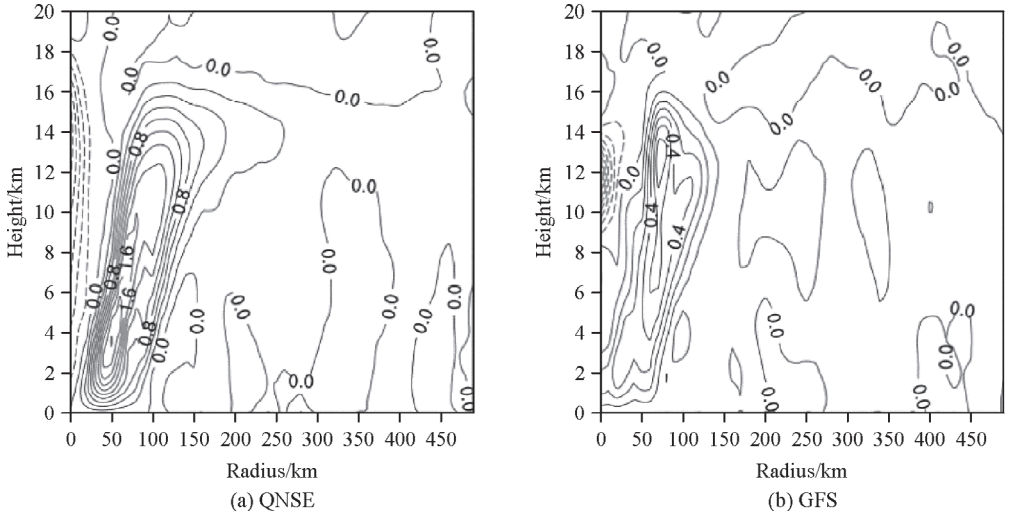

Fig. 9 Simulated azimuthally-averaged vertical velocity (unit: m/s) of TC inner core at 00:00 on 13 September, 2018 at radius-height.

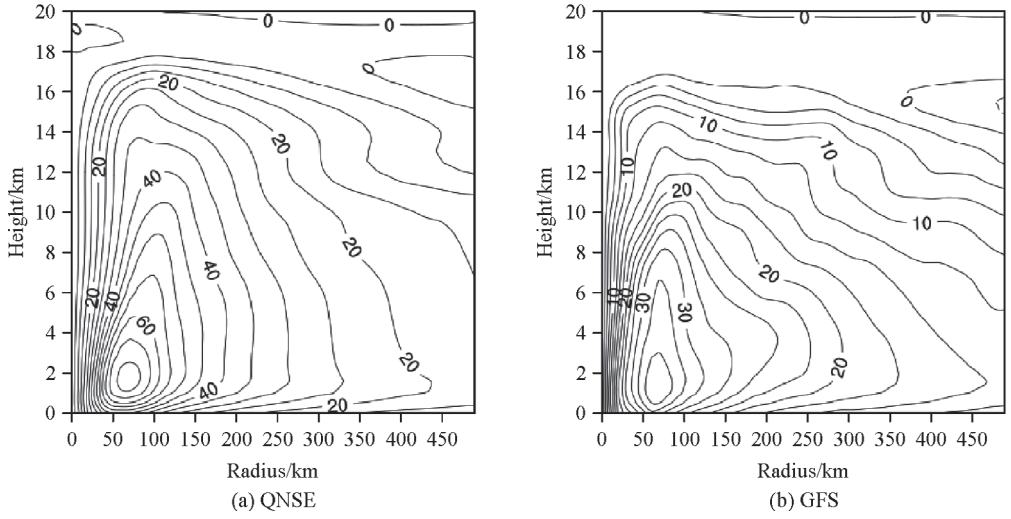

Fig. 10 Simulated azimuthally-averaged tangential wind speed (unit: m/s) of TC inner core at 00:00 on 13 September, 2018 at radius-height.

circulation of the typhoon was simulated higher than that in QNSE scheme. The strongest tangential wind was found at the radius of 60 km in the two experiments. However, the simulated tangential wind was much stronger in QNSE-EXP than that in GFS-EXP, with the maximum tangential speed of 70 m/s and 35 m/s, respectively. In addition, the circulation gradient was much larger in QNSE-EXP than that in GFS-EXP, showing a more compact distribution, which just confirmed that the typhoon structure was simulated compact by QNSE scheme and loose by GFS scheme (Fig. 6).

The radial wind reflected the convergence and divergence of the high and low layers of the typhoon. As can be seen from Fig. 11, convergence was basically at the lower layer below 2 km while divergence was basically at the upper layer above 2 km. The strongest outflow airflow was at the upper layer. Due to the inclination of the deep convection in the wall region of the typhoon eye, divergence was corresponding to the vertical rise region of the eyewall. In the simulation using the QNSE scheme, the strongest inlet airflow was 28 m/s near the surface and the strongest outlet airflow was 32 m/s at the height of 16 km. However, the radial wind in GFS-EXP was much weaker than that in QNSE-EXP. The strongest inlet airflow was 8 m/s near the surface and outlet flow was 10 m/s at the height of 15 km. Therefore, both the low inlet flow and the high outlet flow were simulated stronger in QNSE-EXP, which was consistent with the simulated typhoon intensity.

The radar reflectivity factor simulated by the two schemes were both minimized at the typhoon center (Fig. 12), then gradually increased, reached the maximum in the eyewall region, and then weakened outwardly. Over

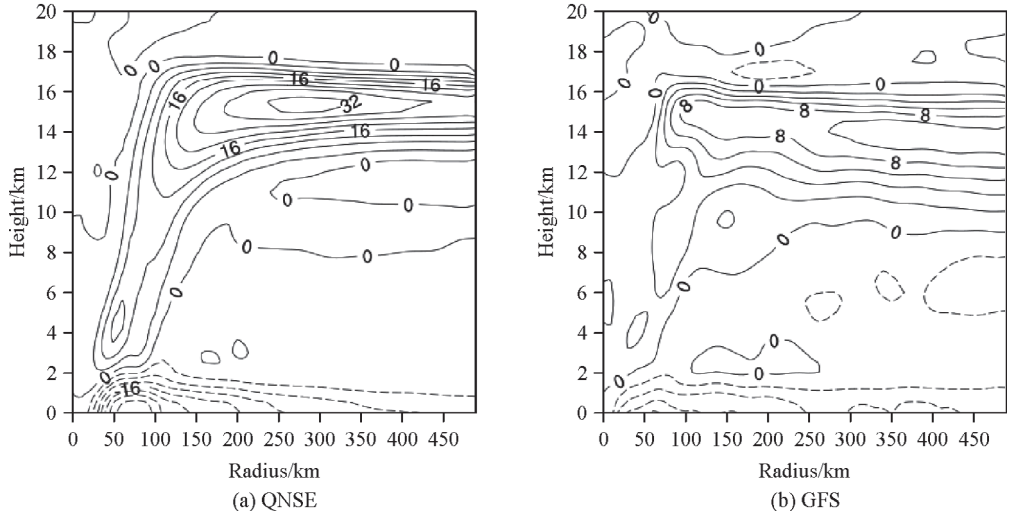

Fig. 11 Simulated azimuthally-averaged radial wind speed (unit: m/s) of TC inner core at 00:00 on 13 September, 2018 at radius-height.

time, the value of the strongest radar reflectivity factor in QNSE-EXP increased rapidly, at 06:00 on 12 September, the simulated strongest reflectivity was over 48 dBz. The strongest region gradually moved toward the typhoon center. The intensity of the radar reflectivity factor in GFS-EXP did not change much over time. The simulated strongest reflectivity factor was 40 dBz. The region with the strongest reflectivity factor was gradually moving closer to the typhoon center. The radar reflectivity factor increased faster in QNSE-EXP than that in GFS-EXP, which was consistent with Figs. 3 and 4 that the typhoon intensity was simulated faster and stronger by the QNSE scheme than by the GFS scheme during this stage.

In the stage of the rapid intensification of the typhoon, the typhoon center was basically a sinking movement (Fig. 13), while the rest of the region was dominated by an ascending movement. Using the QNSE scheme, the strongest updraft was basically at the radius of 50 km, which was weak in the early stage and increased slowly at 12:00 on 10 September 2018, then decreased, and increased from 18:00 on 10 September, until it reached its maximum. The variation trend was basically consistent with the variation trends of the surface fluxes and the PBL height (Fig. 5). The downdraft was simulated significantly weaker using the GFS scheme than using the QNSE scheme. The updraft was simulated also weaker using the GFS scheme than using the QNSE scheme in most periods until the strong updraft began to appear at the radius of 50 km at 12:00 on 11 September 2018. It is shown that in the stage of the rapid intensification of the typhoon, the convection activity in QNSE-EXP was always stronger than that in GFS-EXP, so the typhoon was strengthened faster and stronger using the QNSE scheme.

The tangential velocity in both simulations increased rapidly over time. However, the increase rate was larger and the tangential wind intensity was stronger using the QNSE scheme (Fig. 14). The simulated tangential velocity using the QNSE scheme was 2 times more than that using the GFS scheme. The maximum tangential wind in QNSE-EXP was mainly located at the radius of 50 km during the rapid intensification stage. The maximum tangential wind in GFS-EXP was slowly approaching the typhoon center over time, located within the radius of 50–200 km. Over time, the tangential velocity gradient of typhoon periphery gradually increased, reflecting the characteristics of rapid strengthening and gradually compact structure. However, this change was more obvious using the QNSE scheme than using the GFS scheme, which was consistent with the conclusion that simulation of typhoon structure using QNSE scheme was more compact.

The radial wind simulated had inflow airflow in the typhoon center and outflow airflow in the remaining areas (Fig. 15). The radial and vertical velocities (Fig. 13) of the typhoon in QNSE-EXP were similar. There were negative values were in the typhoon center and positive values in the eyewall region. After a peak at 12:00 on 10 September, they weakened and began to strengthen at 18:00 on 10 September. The large value region did not move with time. However, the large value region of the radial velocity was located near the radius of 150 km, which was further from the typhoon center than the large value region of vertical velocity. At the early stage of strengthening, the simulated radial wind using the GFS scheme had the characteristics of daily variation in the process of intensification: after 00:00 on the 12th, the radial wind increased rapidly and reached the strongest at 18:00 on the 12th. In the early

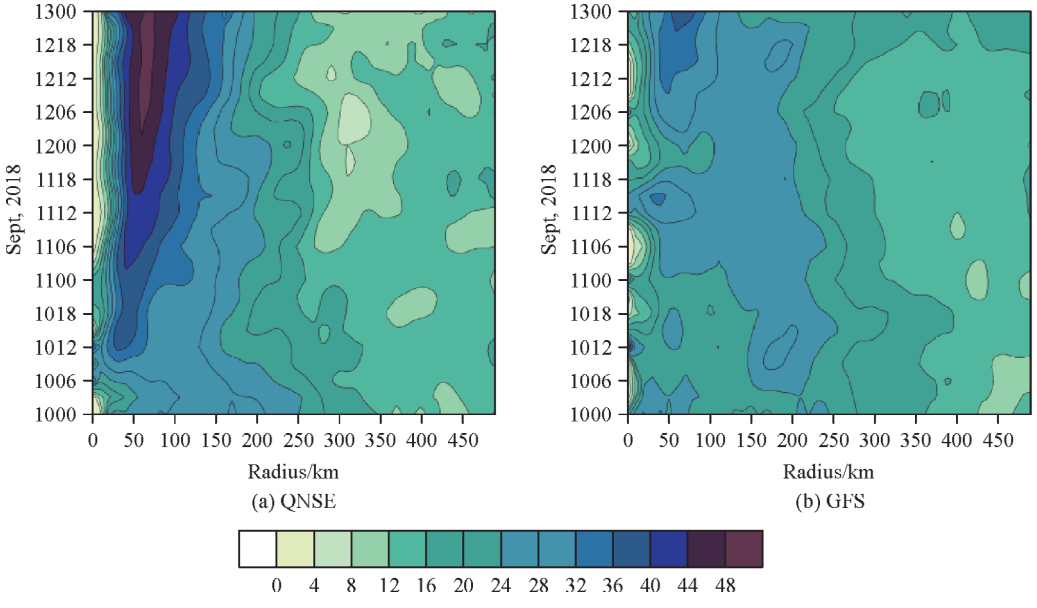

Fig. 12 Simulated time variation of vertical-averaged and azimuthally-averaged radar reflectivity factor (unit: dBz) of TC inner core during the rapid intensification stage.

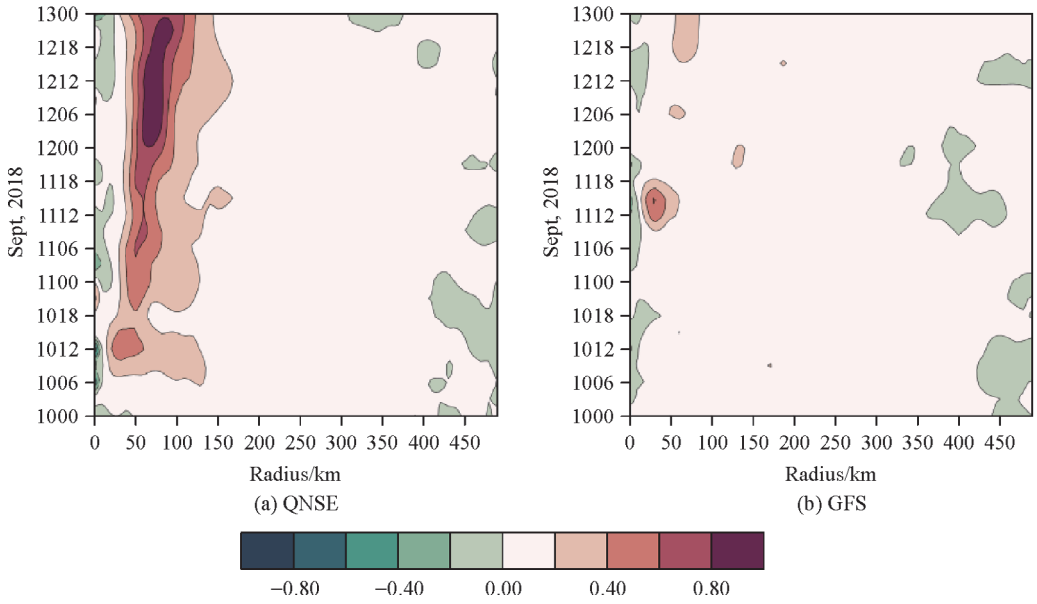

Fig. 13 Simulated time variation of vertical-averaged and azimuthally-averaged vertical velocity (unit: m/s) of TC inner core during the rapid intensification stage.

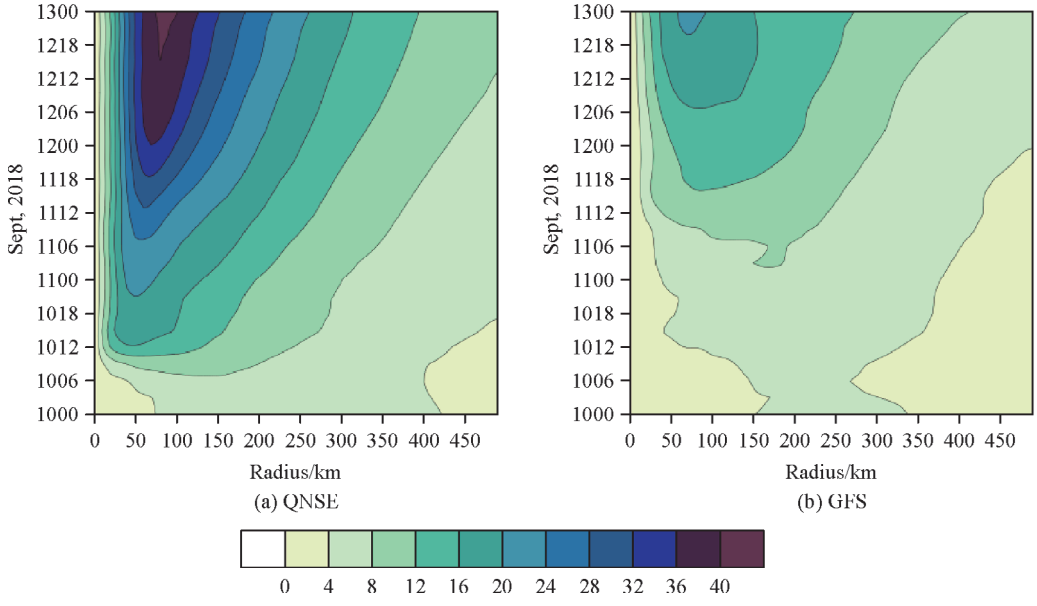

Fig. 14 Simulated time variation of vertical-averaged and azimuthally-averaged tangential wind speed (unit: m/s) of TC inner core during the rapid intensification stage.

stage of typhoon intensification, the large value area of the radial velocity simulated by GFS scheme was located near the typhoon radius of 250 km. Then, it slowly approached to the typhoon center, arrived near the typhoon radius of 200 km at 12:00 on 11 September, and then gradually moved outward. As a whole, the radial velocity simulated by QNSE scheme was significantly larger than that simulated by GFS scheme.

6 Conclusions and discussion

Local closure QNSE and non-local closure GFS PBL schemes were selected to simulate super typhoon Mangkhut (2018), and both PBL schemes had corresponding surface layer schemes, which provided calculation methods of surface fluxes. The spatial resolution was 3 km and the simulation duration was 10.5 days. The track

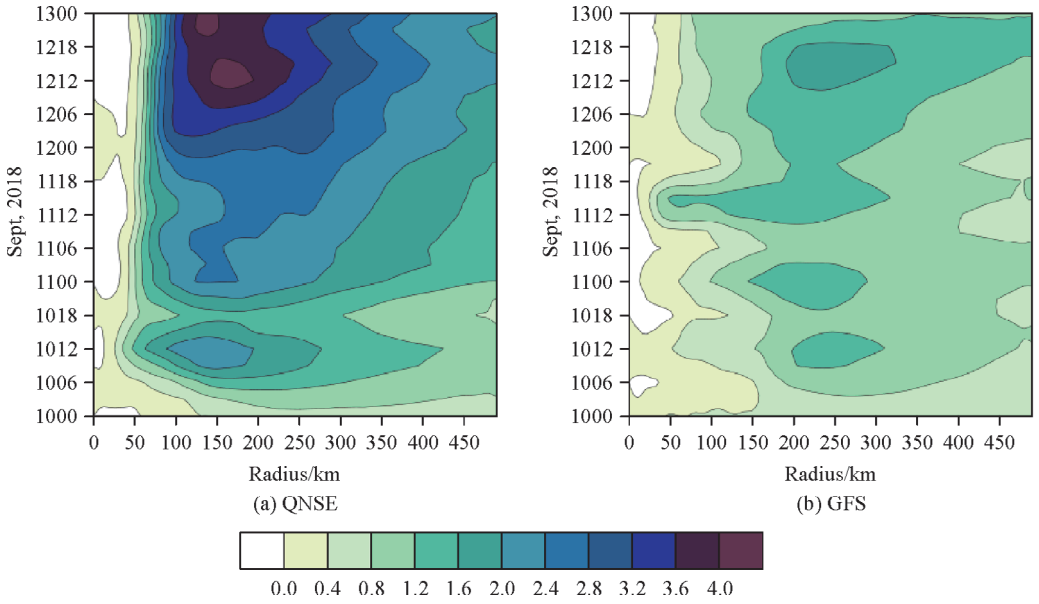

Fig. 15 Simulated time variation of vertical-averaged and azimuthally-averaged radial wind speed (unit: m/s) of TC inner core during the rapid intensification stage.

and intensity simulation results of the typhoon were compared with the observations. Further analysis was conducted for simulation results using the two schemes on the characteristics of the typhoon surface fluxes and vertical structure. Following conclusions were drawn.

With the comparison between the simulation and observation on typhoon track, intensity, error graphs, and error statistics, both PBL schemes can well reproduce the track and intensity of this typhoon. Simulated intensity was weaker than that of the best track data, in which the track and intensity of Typhoon Mangkhut in QNSE-EXP were relatively closer to the observations. Local and non-local PBL schemes had a large influence on both the intensity and the structure of typhoon. The simulated minimum sea level pressure using QNSE scheme was 50 hPa lower than that using the GFS scheme.

Based on the research and analysis on the surface fluxes and the vertical structure of the typhoon, it is found that the simulated typhoon in QNSE-EXP test has larger surface latent heat flux, surface sensible heat flux, and surface vapor flux than those simulated with GFS scheme. Larger surface fluxes provides more energy, leading to a stronger typhoon. Therefore, the intensity of typhoon simulated with QNSE-EXP scheme was stronger than that with GFS-EXP. The largest flux was latent heat flux, as the main source of typhoon energy. Due to different surface layer schemes, the surface fluxes were simulated significantly in two experiments. The differences caused by surface layer schemes is dominant among the differences between the two simulations. The typhoon in QNSE-EXP had a larger surface friction velocity which induced stronger turbulent mixing. Its PBL height was also higher, leading the energy to reach a higher level, hence the typhoon had more energy. In QNSE-EXP, the tangential velocity was larger and the flow into the lower layer and out of the upper layer was stronger than those by the GFS scheme, so the typhoon intensity in QNSE-EXP was stronger than that by the GFS scheme. The latent heat flux and sensible heat flux on the surface conveyed energy upward for the typhoon, and water vapor was transported upward through vertical mixing. As the water vapor condensed, the latent heat was released, which warmed the typhoon eyewall, providing energy for the convection.

In the stage of rapid intensification, the surface latent heat flux, sensible heat flux, water vapor flux, and boundary layer height in QNSE-EXP showed a trend of rapid increase overall and a trend of slow increase in GFS-EXP. And the QNSE scheme had stronger vertical mixing, conveying more energy and water vapor in the typhoon. The radar reflectivity factor, convective activity, and circulation intensity in QNSE-EXP in the region of the wind and eyewall were also stronger and intensified more rapidly.

The case studied in this paper showed that the typhoon track and the intensity simulated by the local QNSE scheme were superior to that by the non-local GFS scheme. In the rapid intensification stage, the typhoon simulated by QNSE scheme has a larger friction velocity, a higher PBL height, stronger vertical mixing, and thus stronger intensity and less deviation to the observation. It is well known that sensitivity studies are case-dependent. There are many factors influencing typhoon intensity, such as model resolution and other physical processes (Sun et al., 2013; Li et al., 2009, 2013, 2020). More case studies are needed

to verify the mechanism of the PBL scheme affecting the typhoon track and intensity.

Acknowledgements This study was funded by the National Key Research and Development Program of China (No. 2016YFA0602701), the National Natural Science Foundation of China (Grant Nos. 42075064 and 41875168), Guangdong Province Key Laboratory for Climate Change and Natural Disaster Studies (No. 2020B1212060025), and this work was supported by the Jiangsu Collaborative Innovation Center for Climate Change.

References

Bae S Y, Hong S Y, Tao W K (2019). Development of a single-moment cloud microphysics scheme with prognostic hail for the Weather Research and Forecasting (WRF) model. Asia-Pac J Atmos Sci, 55 (2): 233–245

Braun S A, Tao W K (2000). Sensitivity of high-resolution simulations of hurricane Bob (1991) to planetary boundary layer parameterizations. Mon Weather Rev, 128(12): 3941–3961

Deng G, Zhou Y S, Li J T (2005). The experiments of the boundary layer schemes on simulated typhoon Part I: the effect on the structure of typhoon. Chinese J Atmos Sci, 29(3): 417–428 (in Chinese)

Ding C H, Li J N, Zhao Y J, Feng Y R (2018). The influence of boundary layer parameterization schemes on autumn typhoon Sarika (2016) in South China Sea. J Tropical Meteorology, 34(5): 657–673 (in Chinese)

Deardorff J W (1972). Theoretical expression for the countergradient vertical heat flux. J Geophys Res Atmos, 77(30): 5900–5904

Dudhia J (1989). Numerical study of convection observed during the Winter Monsoon Experiment using a mesoscale two–dimensional model. J Atmos Sci, 46(20): 3077–3107

Efstathiou G A, Zoumakis N M, Melas D, Lolis C J, Kassomenos P (2013). Sensitivity of WRF to boundary layer parameterizations in simulating a heavy rainfall event using different microphysical schemes. Effect on large-scale processes. Atmos Res, 132(10):125–143

Emanuel K A (1995). Sensitivity of tropical cyclones to surface exchange coefficients and a revised steady-state model incorporating eye dynamics. J Atmos Sci, 52(22): 3969–3976

Filippos T, Demetris C, Silas M, Jos L (2018). Intercomparison of boundary layer parameterizations for summer conditions in the eastern Mediterranean island of Cyprus using the WRF-ARW model. Atmos Sci, 208: 45–59

Holtslag A A M, Boville B A (1993). Local versus non-local boundary layer diffusion in a global climate model. Climate (Basel), 6(10): 1825–1842

Holtslag A A M, Moeng C H (1991). Eddy diffusivity and counter-gradient transport in the convective atmospheric boundary layer. J Atmos Sci, 48(14): 1690–1698

Hong S Y, Pan H L (1996). Non-local boundary layer vertical diffusion in a medium-range forecast model. Mon Weather Rev, 124(10): 2322–2339

Huang W Y, Shen X Y, Wang W G, Huang W (2014). Comparison of the thermal and dynamic structural characteristics in boundary layer with different boundary layer parameterizations. Chinese J Geophys, 57(5):1399–1414 (in Chinese)

Janjić Z I (2002). Nonsingular implementation of the Mellor—Yamada level 2.5 scheme in the NCEP Meso model. NCEP Office Note

Kaplan J, DeMaria M (2003). Large-scale characteristics of rapidly intensifying tropical cyclones in the North Atlantic basin. Weather Forecast, 18(6): 1093–1108

Li J N, Ding C H, Li F Z, Chen Y L (2020). Effects of single- and double-moment microphysics schemes on the intensity of super typhoon Sarika (2016). Atmos Res, 238: 104894

Li J N, Huang X D, Wang G, Fong S K, Li W B (2009). Numerical simulation study of the inner-core structures and the mechanism for inshore strengthening of South China Sea Typhoon Vongfong (0214) during landfall. J Trop Meteorol, 15(1): 45–48

Li J N, Wang G, Lin W S, He Q H, Feng Y R, Mao J Y (2013). Cloud-scale simulation study of Typhoon Hagupit (2008) Part II: Impact of cloud microphysical latent heat processes on typhoon intensity. Atmos Res, 120: 202–215

Liu J J, Zhang F M, Pu Z X (2017). Numerical simulation of the rapid intensification of Hurricane Katrina (2005): Sensitivity to boundary layer parameterization schemes. Advances in Atmos Sci, 34(4): 482–496

Li X L, Pu Z X (2008). Sensitivity of numerical simulation of early rapid intensification of Hurricane Emily (2005) to cloud microphysical and planetary boundary layer parameterizations. Mon Weather Rev, 136 (12): 4819–4838

Mellor G L, Yamada T (1982). Development of a turbulence closure model for geophysical fluid problems. Rev Geophys Space Phys, 20 (4): 851–875

Ming J, Zhang J A (2016). Effects of surface flux parameterization on the numerically simulated intensity and structure of Typhoon Morakot (2009). Advances in Atmos Sci, 33: 58–72

Mlawer E J, Taubman S J, Brown P D, Iacono M J, Clough S A (1997). Radiative transfer for inhomogeneous atmospheres: RRTM, a validated correlated-k model for the longwave. J Geophys Res, 102 (D14): 16663–16682

Moss M S, Rosenthal S L (1975). On the estimation (from bulk data) of boundary layer variables and cloud base mass flux in mature hurricanes. Mon Weather Rev, 20(4): 851–875

Nolan D S, Zhang J A, Stern D P (2009a). Evaluation of planetary boundary layer parameterizations in tropical cyclones by comparison of in situ observations and high-resolution simulations of Hurricane Isabel (2003). Part I: initialization, maximum winds, and the outer-core boundary layer. Mon Weather Rev, 137(11): 3651–3674

Nolan D S, Zhang J A, Stern D P (2009b). Evaluation of planetary boundary layer parameterizations in tropical cyclones by comparison of in situ observations and high-resolution simulations of Hurricane Isabel (2003). Part Ⅱ: inner-core boundary layer and eyewall structure. Mon Weather Rev, 137(11): 3675–3698

Pleim J E, Chang J S (1992). A non-local closure model for vertical mixing in the convective boundary layer. Atmos Environ, 26A(6): 965–981

Ricchi A, Miglietta M M, and et al. (2017). Sensitivity of a Mediterranean tropical-like cyclone to different model configurations and coupling strategies. Atmosphere, 8(5): 92

Rotunno R, Bryan G H (2012). Effects of parameterized diffusion on simulated hurricanes. J Atmos Sci, 69(7): 2284–2299

Smith R K, Thomsen G L (2010). Dependence of tropical-cyclone intensification on the boundary-layer representation in a numerical model. Quarterly J Royal Meteorol Soc, 136(652): 1671–1685

Sukoriansky S, Galperin B, Perov V (2005). Application of a new spectral model of stratified turbulence to the atmospheric boundary layer over sea ice. Boundary-Layer Meteorol, 117(2): 231–257

Sun W Q, Li C Y (2018). A review of atmospheric boundary layer parameterization schemes in numerical models. J Marine Meteorology, 38(3): 11–19 (in Chinese)

Sun Y, Yi L, Zhong Z, Hu Y J, Ha Y (2013). Dependence of model convergence on horizontal resolution and convective parameterization in simulations of a tropical cyclone at gray-zone resolutions. J Geophys Res, 118(14): 7715–7732

Tewari M F, Chen W, Wang J, Dudhia J, Cuemca R H (2004). Implementation and verification of the unified NOAH land surface model in the WRF model. In: 20th Conference on Weather Analysis and Forecasting/16th Conference on Numerical Weather Prediction: 11–15.

Troen I B, Mahrt L (1986). A simple model of the atmospheric boundary layer; sensitivity to surface evaporation. Boundary-Layer Meteorol, 37:129–148

Tymvios F, Demetris C, Silas M, Jos L (2018). Intercomparison of boundary layer parameterizations for summer conditions in the eastern Mediterranean island of Cyprus using the WRF-ARW model. Atmos Res, 208: 45–59

Wang Y X, Zhong z, Sun Y, Hu Y J (2017). The mechanism analysis of the track deviation of tropical cyclone Megi (2010) simulated with two planetary boundary layer schemes. Chinese J Geophy, 60(7): 2545–2555 (in Chinese)

Wen X P, Long X, Zhang S W, Li D H (2018). Numerical studies of planetary boundary layer parameterization schemes on super typhoon SANBA (2012) during its initial stage. J Trop Meteorol, 24(3): 288–299

Xu H Y, Xu Y Q, Wang Z, Zhu P J, Li X F, Zhai G Q (2017). Modification tests for the coefficient of turbulent mixing length scale in QNSE scheme in the WRF model. Chinese J Atmos Sciences, 41 (2): 357–371 (in Chinese)

Yamada T, Mellor G L (1975). A simulation of the Wangara atmospheric boundary layer data. J Atmos Sci, 32: 2309–2329

Ying M, Zhang W, Yu H, Lu X Q, Feng J X, Fan Y X, Zhu Y T, Chen D Q (2014). An overview of the China Meteorological Administration tropical cyclone database. J Atmos Ocean Technol, 31(2): 287–301

Zhang Y T, Jiang Y X, Tan B K (2013). Influences of different PBL schemes on secondary eyewall formation and eyewall replacement cycle in simulated Typhoon Sinlaku (2008). Acta Meteorol Sin, 27 (3): 322–334

Zhang J A, Rogers R F, Tallapragada V (2017). Impact of parameterized boundary layer structure on tropical cyclone rapid intensification forecasts in HWRF. Mon Weather Rev, 145: 1413–1426